Research Square

Preprints are preliminary reports that have not undergone peer review.
They should not be considered conclusive, used to inform clinical practice,
or referenced by the media as validated information.

Polylactic acid/kenaf cellulose biocomposite filaments for melt extrusion based-3D printing

Chuanchom Aumnate (chuanchom.a@chula.ac.th)
Chulalongkorn University https://orcid.org/0000-0003-4377-333X
Niphaphun Soatthiyanon
Chulalongkorn University
Thidarat Makmoon
National Science and Technology Development Agency
Pranut Potiyaraj
Chulalongkorn University

Original Research

Keywords: 3D printing, kenaf cellulose, polylactic acid, biocomposites

Posted Date: February 24th, 2021

DOI: https://doi.org/10.21203/rs.3.rs-188812/v1

License: This work is licensed under a Creative Commons Attribution 4.0 International License.
Read Full License

Version of Record: A version of this preprint was published at Cellulose on July 9th, 2021. See the published version at https://doi.org/10.1007/s10570-021-04069-1.

Abstract

This study fabricated polylactic acid (PLA)/kenaf cellulose fiber biocomposite filaments via melt-extrusion process. Kenaf cellulose fibers (KF) were chemically extracted from locally grown kenaf plants and used as reinforcement. Moreover, the KF was then treated with tetraethyl orthosilicate (TEOS), so-called KFs, to improve the compatibility between the fibers and PLA matrix. Also, the plasticizers (polyethylene glycol) were incorporated to enhance the flowability and processability of the biocomposites. The melt viscosities of the biocomposites increased as the solid KF and KFs were loaded. However, they were significantly decreased with the addition of plasticizers. The combined use of the plasticizers and TEOS treatment improved tensile strength, Young's modulus and elongation of the biocomposites compared to the neat PLA. The obtained PLA/KFs biocomposite materials are proved to be a mechanical-improved material, which offers the opportunity for customized and rapid prototyping of biocomposite products.

1. Introduction

Polymer composites have achieved attractive interests over the years for numerous applications and industries such as automotive, aerospace, and biomedical applications. Additive manufacturing or 3D printing evolves a new dimension for composite manufacturing. The simple and low-cost 3D printing technique, Fused Deposition Modeling (FDM), has become the most attractive manufacturing process for composite materials. Polylactic acid (PLA) has recently been considered a replacement for petroleum-based polymers and has been widely used in 3D printing applications. It possesses remarkable properties, including renewability, biocompatibility, biodegradability, and good thermomechanical properties. PLA has been exploited in various fields regarding such moral properties, such as biomedical, drug-eluting systems and also automotive areas. However, there are some drawbacks concerning its brittleness, slow crystallization, and low glass transition temperature. Preparing PLA composites with some fillers and reinforcement materials promotes efforts to overcome these limitations of PLA and match the end properties (Ding et al. 2016; Scaffaro et al. 2017; Mokhena et al. 2018; Aumnate et al. 2021). Natural fibers and particles such as cellulose, silica, and clay have been recognized as feasible additives for enhancing the properties of polymer composites (Jiang et al. 2020). 3D printing of polymer composites become a new approach to achieve a system with more useful structural or functional properties. One common drawback of FDM 3D printing is that the composite materials have to be in a filament form to enable extrusion. It is challenging to achieve homogeneous reinforcement dispersion to diminish the void formation during the FDM 3D printing process, which causes low mechanical properties. Thus, one approach to preparing cellulose composite filaments is to improve the mechanical properties (Wang and Gardner 2017; Tekinalp et al. 2019; Sharma et al. 2020). PLA/microcrystalline cellulose (MCC) composite filaments were found to be successfully prepared using polyethylene glycol (PEG) and silane coupling agent (KH-550) as a plasticizer and a surface modification agent, respectively. (Murphy and Collins 2018). Moreover, a novel 3D printable biocomposite filament produced from wood hemicellulose and PLA was successfully 3D printed as scaffold prototypes. Also, there was a report on

successfully preparing the biocompatible hydroxypropyl-methylcellulose/PLA composite filaments for the FDM 3D printing method (Jiang et al. 2020). The use of the 3D printing technique for fabricating biocomposites could potentially boost the biocomposites in several applications, including tissue engineering and drug delivery system (Xu et al. 2018).

However, there has been a limited amount of research conducted to develop polymer composites for the FDM process, especially the studies carried out involving cellulose-based composites (Murphy and Collins 2018; Chang et al. 2019). Cellulose, natural raw material, has a nearly perfect inerratic structure with good mechanical properties. It was used as a fiber enhancer or reinforcement in polymer composites. The enhancing effect was controlled by its sizes, morphology and structure. The smaller size of the cellulose can enhance the mechanical properties, and the larger size of the cellulose could provide good formability, network structure and entities (Thakur et al. 2014; Gemmeke et al. 2019; Bhasney et al. 2020). In general, cellulose and cellulose derivatives cannot be 3D printed directly. Thus, they are normally prepared as polymer/cellulose composites before manufactured by 3D printing technique. Even though incorporating cellulose into plastic filaments will increase the proportion of biodegradable or renewable raw materials, the obtained filaments' properties will be variation. Compounding or blending techniques influence the dispersion and properties of cellulose/polymer composites significantly. In situ polymerization, melt compounding and solvent blending are the three most commonly used blending techniques for polymer composites. As stated in several studies, melt compounding or melt extrusion techniques are the most common methods in making well-dispersed polymer-based composites (Pinto et al. 2013).

Compatibilizer, such as maleic anhydride, is proposed to enhance the interfacial adhesion and cellulose dispersion in the PLA matrix (Zhou et al. 2018). Alternatively, surface modification and functionalization are off proposing methods to overcome the poor dispersion issues between cellulose and the polymer matrix. Because of the cellulose's hydrophilic nature, the surface modification is targeting to reduce the hydroxyl interactions, which further increase the compatibility with hydrophobic polymeric materials (Frone et al. 2013; Murphy and Collins 2018). Cellulose can be modified with silane derivatives to use as a reinforcement in green polymer composites potentially. Such modification significantly affected their physio-chemical properties, including structural, thermal, and morphological characteristics (Frone et al. 2013; Thakur et al. 2014). As mentioned, the main challenge is to promote the homogeneous dispersion of cellulose in polymer matrixes. Thus, the improvements of interfacial adhesion between cellulose and polymer matrixes are required. Interestingly, the cellulose surface modification with tetraethyl orthosilicate (TEOS) has shown various advantages, including low-temperature processing, controllable of composition, resultant structure, and easy scale-up. Also, it has been devoted much effort to fabricate superhydrophobic surfaces. Cellulose that crosslinked with TEOS can form strengthened cellulosic gels through Si-O joining, resulting in improved thermal properties and hydrophobic characteristics (Fu et al. 2018; Xie et al. 2019; Zhang et al. 2019). Moreover, the plasticizers and coupling agents can be incorporated into the PLA/cellulose composite system to improve cellulose dispersion due to the long alkyl chain (Immonen et al. 2017).

This study addresses the critical factors in the manufacturing of PLA/kenaf cellulose (locally grown in Thailand) composites by using conventional techniques to generate degradable biocomposites with added value, such as biodegradability and complexity of the geometry and shape of the parts. The effects of surface modification with TEOS and plasticizer addition and the influence of the molecular weight of the plasticizers, are examined. Different aspects, including thermal properties, rheological behaviors, morphology, and mechanical properties of the biocomposites, are also discussed.

2. Experimental

2.1. Materials

Kenaf cellulose fibers (KF) were extracted from the untreated kenaf fibers, Ban Tokpan housekeepers' kenaf fiber weave group in Khon Kean, Thailand. 3D printing monofilament grade polylactic acid (PLA) (Ingeo™ Biopolymer 4043D, NatureWorks), with the MFR of 6.0 g/10min (190°C /2.16 kg) and the density of 1.24 g/cm^3 was used as a matrix polymer. Absolute ethanol (C_2H_5OH) (RPE-ACS grade, CARLO) and tetraethyl orthosilicate ($Si(OC_2H_5)_4$) (reagent grade 98%, Sigma-Aldrich) were used as received. Acetic acid (glacial ≥ 99%, Sigma-Aldrich) was used as a catalyst for TEOS treatment. Polyethylene glycol 4000 (PEG4) and polyethylene glycol 6000 (PEG6) were purchased from Sigma-Aldrich and used as received.

2.2. Kenaf cellulose fiber extraction

Untreated kenaf fibers were treated using 12%w/v NaOH in a 1:20 fiber to liquor ratio, at 80 ± 2^{o}C for 3 h. The treated kenaf fibers were then washed with water and oven-dried. The dried fibers were further treated and bleached in a 50:50 mixture of glacial CH_3COOH and 30%w/v H_2O_2 in a 1:20 fiber to liquor ratio, at 80 ± 2^{o}C for 3 h. The fibers were subsequently washed with water, followed by warm ethanol and they were then ground to obtained kenaf cellulose fibers (KF) (Soatthiyanon et al. 2020).

2.3. Surface modification of kenaf cellulose fibers

An alternative method for preparing the silica layer on the surface of kenaf fibers was the sol-gel process catalyzed by acetic acid. Tetraethyl orthosilicate (TEOS, 1.0 g) was dissolved in 100 ml of absolute ethyl alcohol, followed by adding acetic acid (5.0 vol%) dropwise. The hydrolysis was then conducted at 60^{o}C for 1 h. Then, the KF (20 wt% dispersed in absolute ethyl alcohol) was added to the mixture and further stirred at 60^{o}C for 2 h. The obtained surface modified kenaf cellulose (KFs) was then dried in an oven at 50^{o}C for 24 h.

2.4. Biocomposite filament fabrication

Virgin PLA granules and kenaf cellulose fibers, KF and KFs, were dried in a vacuum oven for 8 h to ensure no moisture content. To fabricate the PLA/kenaf cellulose biocomposite filaments, the dried KF and KFs, were prior mixed with PEG to improve the flowability of the KF and KFs in the PLA matrix. Subsequently, the mixture was then melt compounded with the virgin PLA to get the desired final composition as 10

wt% kenaf cellulose fibers (KF or KFs). The melt compounding process was performed using the microcompounder (Thermo Scientific HAAKE MiniLab II) at 180^{o}C and the screw speed of 40 rpm.

2.5. 3D printing of PLA and PLA/kenaf cellulose biocomposites

The obtained PLA filament and PLA/kenaf cellulose biocomposite filaments were 3D printed using a commercial 3D printer (Wanhao, Duplicator6). All filaments were printed using the same printing conditions, listed in Table 1.

Table 1
Parameters setup for 3D printing of PLA and PLA/kenaf cellulose biocomposites.

Parameter	Unit	Value
Print nozzle diameter	[mm]	0.4
Nozzle temperature	[°C]	190
Building plate temperature	[°C]	60
Layer height	[mm]	0.2
Infill density	[%]	30
Printing speed	[mm/s]	20

2.6. Characterization

2.6.1. Attenuated total reflection Fourier transform infrared spectroscopy (ATR-FTIR)

The extracted kenaf fiber was characterized using ATR-FTIR (Perkin-Elmer spectrometer 100) in the range of 4000 – 500 cm^{-1}.

2.6.2. X-ray diffraction (XRD)

The samples' structural and phase analyses of the samples were implemented using a Bruker X-ray diffractometer. All samples were scanned from 5^{o} to 60^{o} for the 2θ range (40 kV, 40 mA). The crystalline index of kenaf cellulose, C_{Ir}, was calculated using the following equation (Segal equation):

$$C_{Ir}\,(\%) = \frac{[I_{200} - I_{amorph}]}{I_{200}} \times 100$$

1

Where I_{200} is the maximum intensity of cellulose crystalline lattice (200) diffraction (2q = 22.5^o) and I_{amorph} is the intensity of the amorphous fraction (2q = 18.0^o) (Segal et al. 1959; Kargarzadeh et al. 2012; French 2014; Song et al. 2018)

2.6.3 Thermogravimetric analysis (TGA)

Thermal stability data was obtained using the NETZSCH TG 209 F3 thermogravimetric analyser under linear temperature conditions. The samples were heated within the temperature range of 35^{o}C to 600^{o}C at a heating rate of 10^{o}C/min in a nitrogen atmosphere.

2.6.4 Non-isothermal crystallization differential scanning calorimetry

The DSC 3500 Sirius was used to measure the thermal properties of the materials, under nitrogen atmosphere. The filament samples were heated from 30°C to 200°C with the temperature ramp of 10 K/min, and kept isothermal for 2 min. The samples were then cooled down to 30°C with the temperature ramp of 10 K/min. Following by the second heating scan, the samples were again heated up to 200°C and kept isothermal for 2 min with the same temperature ramping. Consequently, the degree of crystallization ( ) of PLA and its composites with kenaf cellulose fiber can be determined based on the following equations (Boruvka et al. 2019)

$$X_c = \frac{\Delta H_m - \Delta H_c}{\Delta H_{mo} \times w} \times 100\%$$

2

Where ΔH_m is the enthalpy of melting and ΔH_c is the enthalpy of crystallization and w the weight fraction of PLA in the sample. ΔH_{mo} is the enthalpy of melting for 100% crystallized PLA, which was taken as 93.1 J/g (Hamad et al. 2015).

2.6.5 Scanning electron microscopy (SEM)

Morphology of the tensile tested specimens of the neat PLA and its biocomposites were examined using a JEOL JSM-IT500HR scanning electron microscope (SEM) at an accelerating voltage of 5 kV. The specimens were sputter coated with gold before the examination.

2.6.6 Rheology

A parallel-disk (1mm gap and diameter of 25 mm) rheometer (Germini 2000, TA instrument) was used for all rheological testing. Based on strain sweeps at 6.28 rad/s, a constant strain amplitude was fixed at 1%,

to ensure linearity. Frequency sweeps from 0.0628 to 628 rad/s were performed at 200°C and fixed strain amplitude at 1%. The corresponding steady shear measurements were also conducted at 200°C, over the range from 0.01 to 1000 s^{-1}.

2.6.7 Tensile testing

The dog bone-shape specimens (Type-V) were printed in accordance with ASTM D638 (American Society for Testing and Material (ASTM) 2014). All tensile tests were performed using a crosshead speed of 5 mm/min. The ultimate tensile strength, Young's modulus and elongation at break of the printed samples were evaluated as averages of at least three replicates.

3. Results And Discussion

3.1. Extracted kenaf cellulose (KF)

The extracted cellulose fibers (KF) used in this study were verified via FTIR spectrum, as shown in Fig. 2(a). The spectrum show the characteristic peaks at 3300–3400 cm^{-1}, attributed to the stretching vibration of the OH groups of cellulose. The C-H stretching vibration at around 2800–2900 cm^{-1}, corresponding to the presence of C-H stretching. The peak at 1420–1430 cm^{-1} and 1300–1400 cm^{-1}, are attributed to the symmetric bending of CH_2 and the bending vibrations of the C-H and C-O groups of the aromatic rings in polysaccharide (Jonoobi et al. 2009; Kargarzadeh et al. 2012). The peak around the range of 1030–1150 cm^{-1}, are attributed to C-O stretching and C-H vibrations of the pyranose ring skeletal. The peak around 895 cm^{-1}, corresponds to COC, CCO, and CCH deformation and stretching vibrations. The FTIR spectrum show that the cellulose was successfully extracted from kenaf fiber.

Figure 2(b) shows the XRD intensities of our extracted kenaf cellulose fiber (Extracted KF) in comparison with commercially available cellulose fiber (Commercial Cellulose). Both cellulose samples presented typical semi-crystalline behavior, in which crystalline peaks at 2θ value of 22.5^{o} were observed. The peaks obtained from the XRD intensities were the characteristic peaks for cellulose. The crystallinity index (CrI) of the commercial cellulose is about 77%, while the CrI of the extracted kenaf cellulose is relatively high at around 71%. Such high CrI of the extracted kenaf cellulose is due to the removal of amorphous hemicellulose and lignin during the bleaching and extraction process (Chan et al. 2013). The XRD results also proved that combined use of low NaOH concentration and relatively low temperature did not alter the cellulose structure compared to the commercially available cellulose.

Furthermore, from our previous study (Soatthiyanon et al. 2020), our extracted cellulose fibers (KF) were found to be decomposed at 337.3^{o}C. The average widths and average length of the extracted kenaf cellulose fibers were 8.9 ± 2.1 μm and 101.7 ± 57.6 μm, respectively, with the aspect ratios of 11.5. The SEM image of the extracted kenaf cellulose fibers was shown in Sect. 3.5 Morphology, Fig. 10(a).

3.2. Thermal properties

The thermal properties of the neat PLA and all the biocomposites, including glass transition temperature (T_g), crystallization temperature (T_c), and melting temperature (T_m) of the PLA and the PLA/KF biocomposites, were characterized using the DSC measurement. The results from the second heating scan and first cooling cycles are shown in Fig. 3. The melting temperature (T_m) of the neat PLA and all the biocomposites remains almost constant at around 151^{o}C, while the glass transition temperature (T_g) is slightly decreased for all the biocomposites with PEG incorporating. This may be attributed to the plasticizer effect of PEG, enhancing the PLA chains' mobility. However, according to the DSC results, it could be concluded that the incorporation of KF, KFs, and PEG showed no significant effect on the melting and the glass transition temperatures of the obtained biocomposites.

For the PLA/KF and PLA/KFs biocomposites, the enhancement of T_c refers to the biocomposite filaments that are more difficult to undergo cold crystallization than the neat PLA filament and thus require higher temperature. As shown in Table 2, the crystallinity of the PLA biocomposites is gradually decreasing with a corresponding decrease in the enthalpy of crystallization as the KF and KFs are adding. However, the addition of PEG seems to diminish the effect of the KF and KFs on decreasing the crystallinity. The crystallinity of the PLA/PEG4/KFs biocomposite remains almost constant while the crystallinity increases for the PLA/PEG6/KFs biocomposite is approximately twofold increased compared to the neat PLA. This may be attributed to the combined effects of the PEG6000 and TEOS modification on improving the PLA chains' mobility, increasing the recrystallization ability (Murphy and Collins 2018).

Table 2
DSC results of PLA and PLA/kenaf cellulose biocomposites.

Sample	T_g [^{o}C]	ΔH_c [J/g]	T_c [^{o}C]	ΔH_m [J/g]	T_m [^{o}C]	X_c [%]
PLA	59.7	16.83	122.2	17.35	150.8	0.56
PLA/KF	59.5	7.28	126.2	7.51	151.3	0.27
PLA/KFs	59.7	6.54	126.8	6.40	151.5	-
PLA/PEG4/KFs	57.9	16.50	122.8	16.98	151.3	0.57
PLA/PEG6/KFs	57.6	16.36	122.7	17.17	151.0	0.97

3.3. Rheological behaviors

Figure 4 shows the complex viscosity (η^*) as a function of angular frequency for the neat PLA and its biocomposites with the kenaf cellulose fibers at 190^{o}C. The complex viscosity increases with the kenaf cellulose fiber addition. This may be attributed to the rigidity of the kenaf cellulose fiber restricted the capability to flow of the melted PLA chains. Remarkably, the surface modification of the kenaf cellulose fibers with TEOS leads to a decrease in the complex viscosity. This may result from the more hydrophobic surfaces of the KFs. The complex viscosities of the PLA/KFs biocomposite were almost similar to those of the neat PLA at all frequencies, which may be attributed to the better dispersion of the KFs in the PLA matrix comparing to the KF. Moreover, the addition of PEG led to a decrease in the complex viscosity

since PEG acts as a plasticizer, enhancing the flowability of the composites. The complex viscosity of the PLA/PEG4/KFs composite was considerably lower than other materials. This might be because the smaller molecule of the PEG4 resulted in a lower viscosity as compare to the larger molecule of the PEG6.

Figure 5. (a) Storage modulus (G') and (b) loss modulus (G") of PLA and its biocomposite filaments at 190^{o}C as a function of angular frequency.

The modulus data is a factor to reveal the molecular rigidity. Figure 5 (a-b) shows the effect of the TEOS modified kenaf cellulose and the PEG addition on the evolution of the storage and loss moduli of the biocomposites. It is seen that the storage moduli increased with increasing the frequencies, which are consistent with the complex viscosity results. The addition of KF increased the storage moduli of the PLA matrix, indicating the effect of the rigidity of the kenaf cellulose fibers. The modified kenaf cellulose (KFs) showed a slight increase in the storage modulus compared to that of the neat PLA. The increase in the storage moduli was more noticeable for the PLA/KF as compared to the other biocomposites. Such an increase in storage moduli indicated that the addition of the KF and KFs resulted in prohibiting the deformation of the PLA chains. However, the presence of the plasticizers, PEG4 and PEG6, reduced the storage moduli at all frequencies. Furthermore, the addition of plasticizers improved the capability to flow of the biocomposites, at the same time, decreased stiffness.

The Cole-Cole plot is generally constructed from the variation in dynamic viscosities, η' and η". It is a useful tool to examine the mechanism of relaxation and homogeneity of polymer composites (Azizi and Ghasemi 2009; Manoharan et al. 2014; Wang et al. 2015; Walha et al. 2016; Aumnate et al. 2019). As shown in Fig. 6, the neat PLA and all the biocomposites present single relaxation behavior. The deviation of semicircular shape means the relaxation process of the PLA/kenaf cellulose biocomposites is affected by the type of the kenaf cellulose (KF and KFs) and the addition of the plasticizers (PEG4 and PEG6). It can be observed clearly that the PLA/KF biocomposite shows the longest relaxation time, in which the most deviation of the semicircular shape from the neat PLA is observed. This behavior indicates the heterogeneity and poor compatibility between the kenaf cellulose fibers (KF) and the PLA matrix. Thus, the motion of PLA chains is restrained significantly. The TEOS modified kenaf cellulose (KFs) enhanced the compatibility between such two phases, the modified kenaf cellulose fibers, and the PLA matrix, leading to improved PLA chain motion, as evidence by the smaller semicircular shape forming.

3.4. Optimization of extrusion-based 3D printing

In melt extrusion-based 3D printing, the crucial parameter to achieve high interfacial bonding between printed layers is the suitable extrusion temperature, in which the molten filament maintains this temperature in the most recently deposited layers. Knowing the extrusion temperature and flowability of the printed materials leads to more accurate and precise printing. The melt viscosity should be adequate to allow extrusion yet sufficient to provide structural support (Aumnate et al., 2018; Wang et al., 2017). Also, a high cooling rate leads to a higher and more uniform mechanical performance. Thus, tuning the cooling rates also matters.

The shear rate for the melt extrusion-based 3D printing processes, in particular the FDM system, is typically ranged between 100 to 200 s^{-1} (Osswald et al. 2013; Aumnate et al. 2019; Spicker et al. 2019). Figure 7 shows the plot of steady shear viscosity versus shear rate for the neat PLA and its composites with the kenaf cellulose fibers. As expected, the viscosity of the biocomposite increases for the PLA/KFs composite. This may be due to the rigidity of the KFs interferes the mobility of the PLA chain. On the other hand, the viscosity of the PLA/KFs composites decreases with the PEG addition. The smaller molecule of PEG4, the lower the viscosity. The reduction in viscosity can be attributed to the plasticizing effect of the PEG, enhancing the flowability of the melt. According to the steady shear viscosity data, over the range of 100 to 200 s^{-1}, the PLA/PEG4KFs biocomposite filament is expected to flow most easily during 3D printing process.

Moreover, the cooling scan from the DSC measurement (see Fig. 1(b)) for the PLA and its biocomposite filaments gives the low bound for the extrusion temperature according to the biocomposite crystallization behavior. Changing in slope indicates the solidification of the materials. The results showed that PLA and all biocomposites were solidified at the temperature below 60°C. The temperature exceeding 60°C will prevent material solidification at the nozzle. Accordingly, a build plate temperature was set at 60°C for the FDM 3D printing test to diminish such shrinkage and warpage.

Figure 8 presents the 3D printed specimens of the PLA, PLA/KF, PLA/KFs, PLA/PEG4/KFs and PLA/PEG6/KFs biocomposites. All the samples were successfully 3D printed using the same printing conditions (see Table 1). The color of the sample deviated upon the material compositions in the biocomposites. The color of the printed biocomposites became lighter as the TEOS modification and plasticizers were presented.

Figure 9. SEM images of the printed samples from (a) PLA, (b) PLA/KF, (c) PLA/KFs, (d) PLA/PEG4/KFs and (e) PLA/PEG6/KFs biocomposites at 100x magnification.

Figure 9 exhibits the SEM micrographs of the fracture surfaces of the printed samples. It is seen that there are some voids appeared in all the samples. Such voids are common for the sample obtained from the melt extrusion based-3D printing due to the lack of molding pressure during the printing process. Moreover, many voids inside the deposited beads were noticed for the PLA/KF biocomposite, resulting from a weak fiber-matrix interfacial adhesion. The inter-bead voids decreased for the PLA/KFs, PLA/PEG4/KFs, and PLA/PEG6/KFs biocomposites. This suggests the improvement of interfacial compatibility between the KFs and the PLA matrix. This may be ascribed to the subsequent surface modifying kenaf cellulose with TEOS and incorporating the plasticizers, which can further enhance the fiber-matrix interfacial adhesion, thereby the mechanical performance improved.

3.5. Morphology

Figure 10 shows SEM micrographs of the KF and KFs at a magnification of 1000x. The surfaces of the KFs seemed to be smoother than those of the KF. This could be evidence of the presence of the TEOS layer that enveloped the fiber surfaces for the KFs.

The critical challenge to achieving the transfer of good mechanical properties of single-fiber nanocellulose to the macroscale properties of the polymer nanocomposites is also to obtain well-dispersed hydrophilic-reinforcing nanocellulose in the polymer matrices, but also optimization of the fiber-matrix interface and improved coupling of fiber and polymer for enhanced stress transfer.

Figure 11 shows SEM micrographs of a cross-sectional view of the tensile testing specimens for the neat PLA, PLA/KF, PLA/KFs, PLA/PEG4/KFs, and PLA/PEG6/KFs biocomposites, respectively. A dense structure can be observed for the neat PLA. There were two different failure modes observed from the test samples. The PLA and all the PLA biocomposite with the KFs depicted a ductile structure, as can be seen from the tiny fibrils that appeared in the images, while the PLA/KF biocomposite showed a brittle structure. Also, for the PLA/KF biocomposite, the fiber imprints and gaps between the fibers and the PLA matrix were noticed. This is due to the different polarities of the hydrophilic KF and the hydrophobic PLA matrix. These features indicate poor adhesion between KF and the PLA matrix. This negatively affected the tensile strengths of the biocomposites because the applied stress was challenging to transfer to the fibers. Meanwhile, compared to the PLA/KF biocomposite, the denser structure can be observed for the PLA/KFs, PLA/PEG4/KFs and PLA/PEG6/KFs biocomposites. It reveals that the KFs fibers are embedded and covered by the PLA matrix which suggested the compatibility between the KFs fibers and the PLA matrix. Also, the addition of PEG improves the dispersion of the KFs as can be seen from a smaller sizer of fiber bundle compared to the PLA/KFs biocomposite without PEG. The gaps between the fibers and the PLA matrix seemed to be diminished in the PLA/KFs biocomposite. This can be suggested that the modified kenaf cellulose surface with TEOS reduced the hydrophilicity of the kenaf cellulose fibers, thus increased the compatibility and interfacial adhesion between the kenaf cellulose fiber and the PLA matrix. The morphologies of the composites were found to be directly related to the tensile properties.

3.6. Tensile properties

Figure 12 shows the tensile strength of the PLA and its biocomposites. As expected, the addition of KF shows adverse effects on the mechanical properties. Due to the hydrophilic character of the cellulose, the poor interfacial adhesion and the poor dispersion of the KF in the PLA matrix can be promoted. It is seen that the addition of the KF significantly affected the tensile strength of the biocomposites, As expected, the Young's modulus increased with the KF addition, which is due to the rigidity of the KF. However, the tensile strength and the elongation at break dropped significantly compared to the neat PLA. This can be attributed to the poor adhesion and poor compatibility between hydrophilic KF and the PLA matrix. Consequently, the weak spots would be generated during the tensile test. The TEOS surface modification seem to help on improving the tensile strength and the elongation of the biocomposites. As shown in Fig. 12(d), the elongation of the biocomposites with KFs were in the same level. However, Young's modulus significantly decreased for the PLA/KFs and the PLA/PEG4/KFs. Remarkably, the biocomposite with the KFs and the PEG6 showed significantly improve in the tensile strength. The higher molecular weight PEG6 improved the tensile strength. From this study, the PLA/PEG6/KFs biocomposite shows the most promising property with an improvement in mechanical performance. This might be the combined

effects of the TEOS modifying and the use of an appropriate plasticizer. As shown in Fig. 12, the tensile strength significantly dropped for the PLA/KF biocomposite.

4. Conclusions

Kenaf cellulose fibers extracted from locally grown kenaf plants (KF) are successful in being used as reinforcements in the PLA matrix. This study arrived at a methodology of fabricating good-quality PLA/kenaf cellulose biocomposite filaments for the melt extrusion based-3D printing processes, particularly, FDM 3D printing. The surface modification of the kenaf cellulose fibers with TEOS (KFs) improved the compatibility between the kenaf cellulose fibers and the PLA matrix, thus enhanced the composites' mechanical performance. Overall, the results suggested that the TEOS surface treatment combined with the PEG addition was a promising method to fabricate the PLA/kenaf cellulose biocomposite filaments for the melt extrusion-based 3D printing process. PLA incorporated with 10 wt% KFs did not significantly encounter deterioration in the tensile property of the final product. The incorporation of the KF, KFs, and plasticizers caused no significant effect on the melting and glass transition temperatures of the PLA. In other words, it has little influence on intermolecular interactions or chain flexibility of PLA polymer chain. These biocomposite materials offer the opportunity for customized and rapid prototyping of degradable biocomposite products, which will be further useful in various applications such as biomedical and tissue engineering applications.

Declarations

Acknowledgements

The authors thankfully acknowledge the support from Ratchadapisek Sompote Fund (CU-GR_62_38_62_02), Chulalongkorn University and National Research Council of Thailand (NRCT5-TRG63001-01).

References

1. American Society for Testing and Material (ASTM) (2014) Standard Test Method for Tensile Properties of Plastics (D638-14)
2. Aumnate C, Limpanart S, Soatthiyanon N, Khunton S (2019) PP/organoclay nanocomposites for fused filament fabrication (FFF) 3D printing. Express Polym Lett 13:898–909. https://doi.org/10.3144/expresspolymlett.2019.78
3. Aumnate C, Pongwisuthiruchte A, Pattananuwat P, Potiyaraj P (2018) Fabrication of ABS / Graphene Oxide Composite Filament for Fused Filament Fabrication (FFF) 3D Printing. Adv Mater Sci Eng 2018:. https://doi.org/10.1155/2018/2830437
4. Aumnate C, Potiyaraj P, Saengow C, Giacomin AJ (2021) Reinforcing polypropylene with graphene-polylactic acid microcapsules for fused-filament fabrication. Mater Des 198:109329.

https://doi.org/10.1016/j.matdes.2020.109329

5. Azizi H, Ghasemi I (2009) Investigation on the Dynamic Melt Rheological Properties of Polypropylene/Wood Flour Composites. Polym Compos 429–435. https://doi.org/10.1002/pc
6. Bhasney SM, Kumar A, Katiyar V (2020) Microcrystalline cellulose, polylactic acid and polypropylene biocomposites and its morphological, mechanical, thermal and rheological properties. Compos Part B 184:107717. https://doi.org/10.1016/j.compositesb.2019.107717
7. Boruvka M, Behalek L, Lenfeld P, Ngaowthong C (2019) Structure-related properties of bionanocomposites based on poly (lactic acid), cellulose nanocrystals and organic impact modifier. Mater Technol 34:143–156. https://doi.org/10.1080/10667857.2018.1540332
8. Chan CH, Chia CH, Zakaria S et al (2013) Production and characterisation of cellulose and nano-crystalline cellulose from kenaf core wood. BioResources 8:785–794. https://doi.org/10.15376/biores.8.1.785-794
9. Chang Y, Chen Y, Ning J et al (2019) No Such Thing as Trash: A 3D-Printable Polymer Composite Composed of Oil-Extracted Spent Coffee Grounds and Polylactic Acid with Enhanced Impact Toughness. ACS Sustain Chem Eng 7:15304–15310. https://doi.org/10.1021/acssuschemeng.9b02527
10. Ding W, Jahani D, Chang E et al (2016) Development of PLA/cellulosic fiber composite foams using injection molding: Crystallization and foaming behaviors. Compos Part A Appl Sci Manuf 83:130–139. https://doi.org/10.1016/j.compositesa.2015.10.003
11. French AD (2014) Idealized powder diffraction patterns for cellulose polymorphs. 885–896. https://doi.org/10.1007/s10570-013-0030-4
12. Frone AN, Berlioz S, Chailan J-F, Panaitescu DM (2013) Morphology and thermal properties of PLA – cellulose nanofibers composites. Carbohydr Polym 91:377–384. https://doi.org/10.1016/j.carbpol.2012.08.054
13. Fu J, He C, Wang S, Chen Y (2018) A thermally stable and hydrophobic composite aerogel made from cellulose nanofibril aerogel impregnated with silica particles. J Mater Sci 53:7072–7082. https://doi.org/10.1007/s10853-018-2034-9
14. Gemmeke N, Feldmann M, Heim HP (2019) Processing and characterization of engineering biocomposites based on polybutylenterephthalat (PBT) and polytrimethylentherephthalat (PTT) with regenerated cellulose fibers modified with maleic anhydride grafted polyethylene as a processing agent. Compos Part A Appl Sci Manuf 118:327–335. https://doi.org/10.1016/j.compositesa.2019.01.007
15. Hamad K, Kaseem M, Yang HW et al (2015) Properties and medical applications of polylactic acid: A review. Express Polym Lett 9:435–455. https://doi.org/10.3144/expresspolymlett.2015.42
16. Immonen K, Lahtinen P, Pere J (2017) Effects of Surfactants on the Preparation of Nanocellulose-PLA Composites. 1–13. https://doi.org/10.3390/bioengineering4040091
17. Jiang G, Yang T, Xu J et al (2020) Investigation into hydroxypropyl-methylcellulose-reinforced polylactide composites for fused deposition modelling. Ind Crops Prod 146:112174.

https://doi.org/10.1016/j.indcrop.2020.112174

18. Jonoobi M, Harun J, Shakeri A et al (2009) Chemical composition, crystallinity, and thermal degradation of bleached and unbleached kenaf bast (Hibiscus cannabinus) pulp and nanofibers. BioResources 4:626–639. https://doi.org/10.15376/biores.4.2.626-639
19. Kargarzadeh H, Ahmad I, Abdullah I et al (2012) Effects of hydrolysis conditions on the morphology, crystallinity, and thermal stability of cellulose nanocrystals extracted from kenaf bast fibers. Cellulose 19:855–866. https://doi.org/10.1007/s10570-012-9684-6
20. Manoharan S, Suresha B, Ramadoss G, Bharath B (2014) Effect of Short Fiber Reinforcement on Mechanical Properties of Hybrid Phenolic Composites. 2014
21. Mokhena TC, Sefadi JS, Sadiku ER et al (2018) Thermoplastic processing of PLA/cellulose nanomaterials composites. Polymers (Basel) 10:. https://doi.org/10.3390/polym10121363
22. Murphy CA, Collins MN (2018) Microcrystalline cellulose reinforced polylactic acid biocomposite filaments for 3D printing. Polym Compos 39:1311–1320. https://doi.org/10.1002/pc.24069
23. Osswald TA, Menges G, Manges G (2013) Materials Science of Polymers for Engineers, 3rd edn. Hanser Publishers, Munich Vienna New York
24. Pinto AM, Cabral J, Tanaka DAP et al (2013) Effect of incorporation of graphene oxide and graphene nanoplatelets on mechanical and gas permeability properties of poly(lactic acid) films. Polym Int 62:33–40. https://doi.org/10.1002/pi.4290
25. Scaffaro R, Botta L, Lopresti F et al (2017) Polysaccharide nanocrystals as fillers for PLA based nanocomposites. Cellulose 24:447–478. https://doi.org/10.1007/s10570-016-1143-3
26. Segal L, Creely JJ, Martin AE, Conrad CM (1959) An Empirical Method for Estimating the Degree of Crystallinity of Native Cellulose Using the X-Ray Diffractometer. Text Res J 29:786–794. https://doi.org/10.1177/004051755902901003
27. Sharma S, Singh AA, Majumdar A, Butola BS (2020) Harnessing the ductility of polylactic acid / halloysite nanocomposites by synergistic effects of impact modifier and plasticiser. Compos Part B 188:107845. https://doi.org/10.1016/j.compositesb.2020.107845
28. Soatthiyanon N, Aumnate C, Srikulkit K (2020) Rheological, tensile, and thermal properties of poly(butylene succinate) composites filled with two types of cellulose (kenaf cellulose fiber and commercial cellulose). Polym Compos 1–15. https://doi.org/10.1002/pc.25575
29. Song Y, Jiang W, Zhang Y et al (2018) Isolation and characterization of cellulosic fibers from kenaf bast using steam explosion and Fenton oxidation treatment. Cellulose 25:4979–4992. https://doi.org/10.1007/s10570-018-1916-y
30. Spicker C, Rudolph N, Kühnert I, Aumnate C (2019) The use of rheological behavior to monitor the processing and service life properties of recycled polypropylene. Food Packag Shelf Life 19:174–183. https://doi.org/10.1016/j.fpsl.2019.01.002
31. Tekinalp HL, Meng X, Lu Y et al (2019) High modulus biocomposites via additive manufacturing: Cellulose nanofibril networks as “ microsponges ”. Compos Part B 173:106817. https://doi.org/10.1016/j.compositesb.2019.05.028

32. Thakur KM, Gupta KR, Thakur KV (2014) Surface modification of cellulose using silane coupling agent. Carbohydr Polym 111:849–855. https://doi.org/10.1016/j.carbpol.2014.05.041
33. Walha F, Lamnawar K, Maazouz A, Jaziri M (2016) Rheological, morphological and mechanical studies of sustainably sourced polymer blends based on poly(lactic acid) and polyamide 11. Polymers (Basel) 8:. https://doi.org/10.3390/polym8030061
34. Wang L, Gardner DJ (2017) Effect of fused layer modeling (FLM) processing parameters on impact strength of cellular polypropylene. Polym (United Kingdom) 113:74–80. https://doi.org/10.1016/j.polymer.2017.02.055
35. Wang X, Jiang M, Zhou Z et al (2017) 3D printing of polymer matrix composites: A review and prospective. Compos Part B 110:442–458. https://doi.org/10.1016/j.compositesb.2016.11.034
36. Wang XF, Zhang ZX, Li J, Le et al (2015) Largely improved fracture toughness of an immiscible poly(L-lactide)/ethylene-co-vinyl acetate blend achieved by adding carbon nanotubes. RSC Adv 5:69522–69533. https://doi.org/10.1039/c5ra11192g
37. Xie A, Cui J, Chen Y et al (2019) Surface & Coatings Technology One-step facile fabrication of sustainable cellulose membrane with superhydrophobicity via a sol-gel strategy for efficient oil / water separation. Surf Coat Technol 361:19–26. https://doi.org/10.1016/j.surfcoat.2019.01.040
38. Xu W, Pranovich A, Uppstu P et al (2018) Novel biorenewable composite of wood polysaccharide and polylactic acid for three dimensional printing. Carbohydr Polym 187:51–58. https://doi.org/10.1016/j.carbpol.2018.01.069
39. Zhang L, Zhang Q, Yu J et al (2019) Strengthened cellulosic gels by the chemical gelation of cellulose via crosslinking with TEOS. Cellulose 26:9819–9829. https://doi.org/10.1007/s10570-019-02765-7
40. Zhou L, He H, Li M et al (2018) Enhancing mechanical properties of poly(lactic acid) through its in-situ crosslinking with maleic anhydride-modified cellulose nanocrystals from cottonseed hulls. Ind Crop Prod 112:449–459

Figures

Image not available with this version

Figure 1

Figure not available in this version

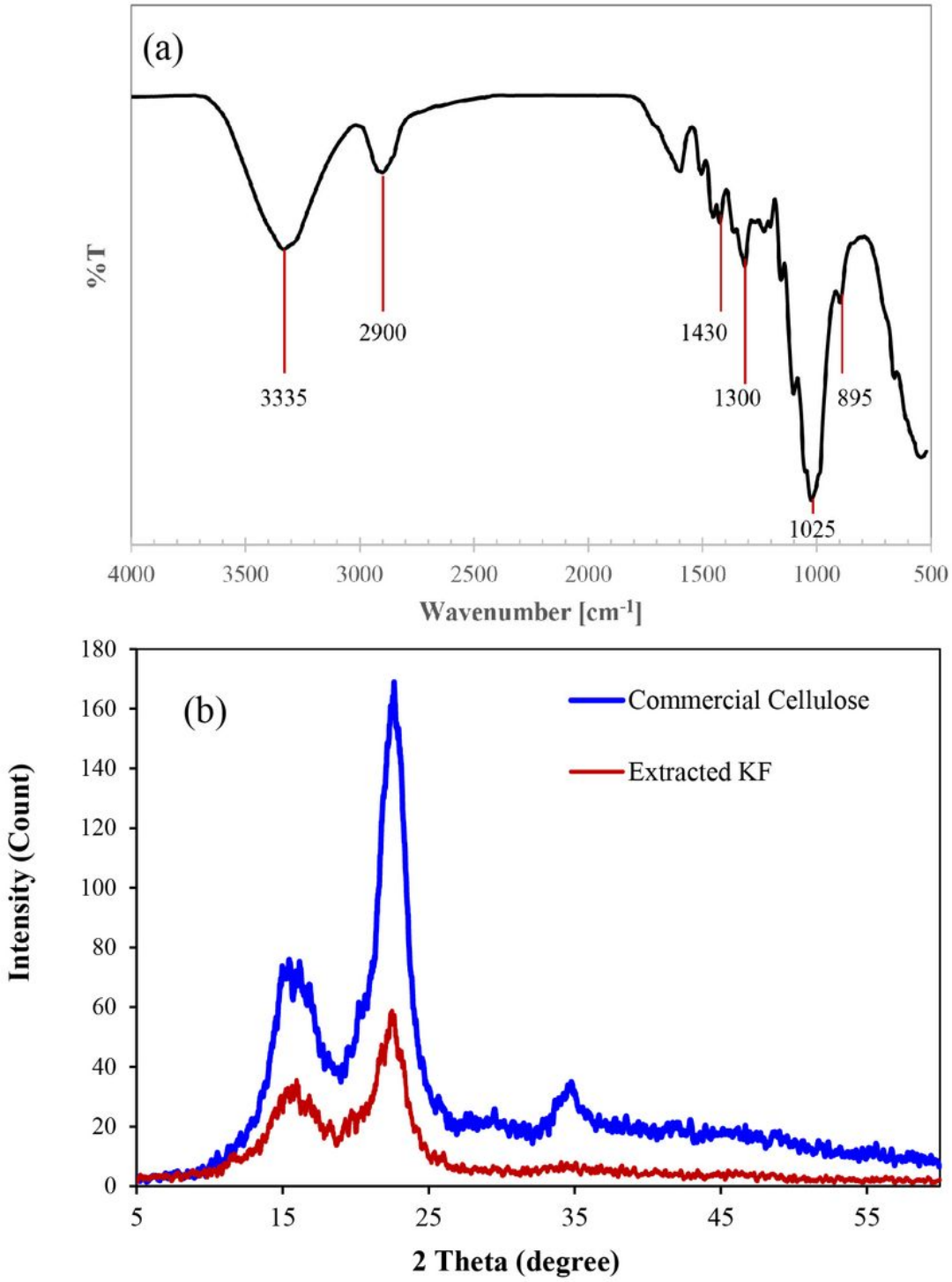

Figure 2

(a) ATR-FTIR spectrum of extracted cellulose fibers (KF) and (b) XRD patterns of commercial cellulose and extracted KF.

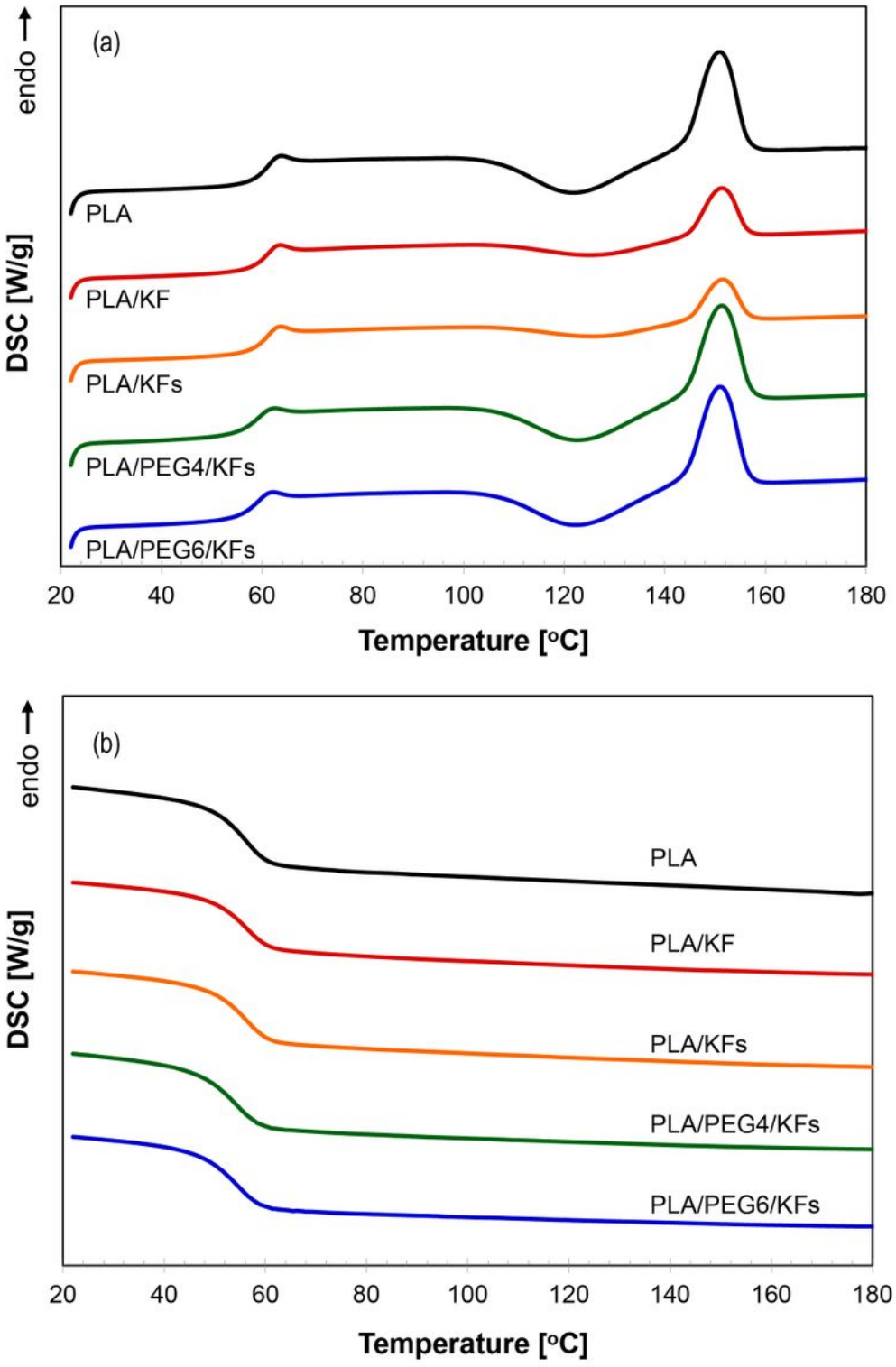

Figure 3

DSC thermograms of (a) the second heating scan, (b) the cooling scan of PLA and its biocomposite filaments.

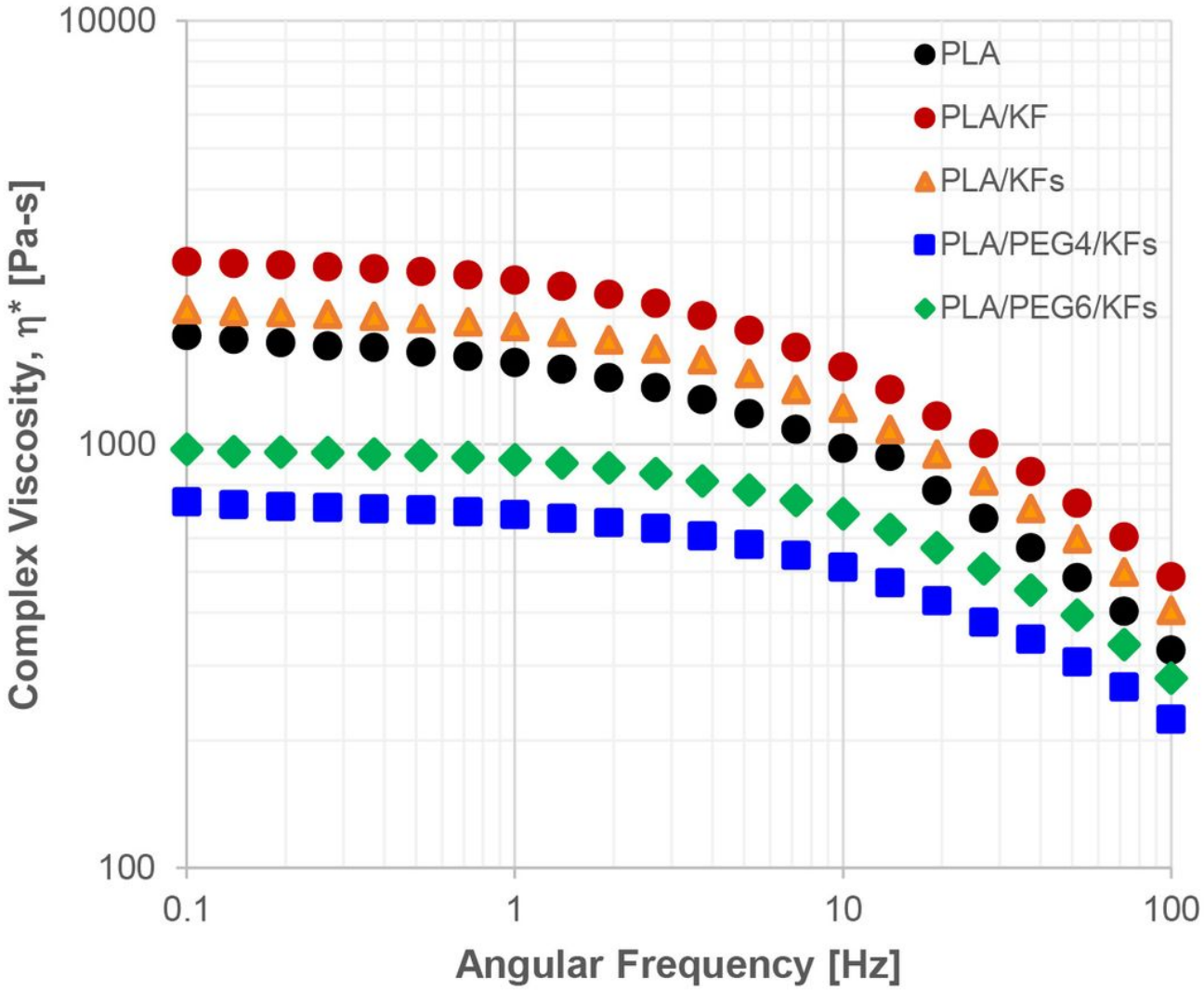

Figure 4

Complex viscosity (η*) of PLA and its biocomposite filaments at 190 oC as a function of angular frequency.

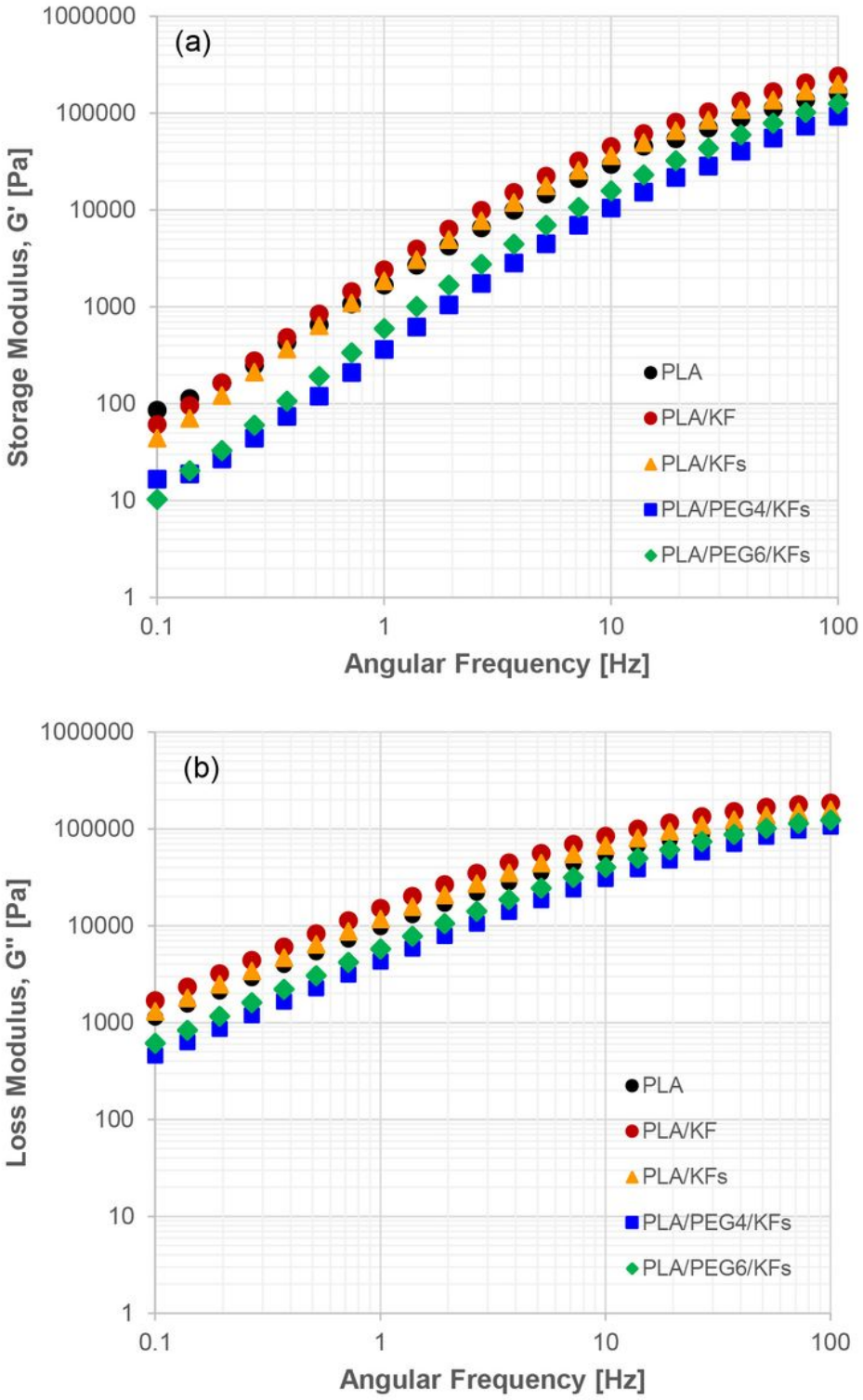

Figure 5

(a) Storage modulus (G') and (b) loss modulus (G") of PLA and its biocomposite filaments at 190oC as a function of angular frequency.

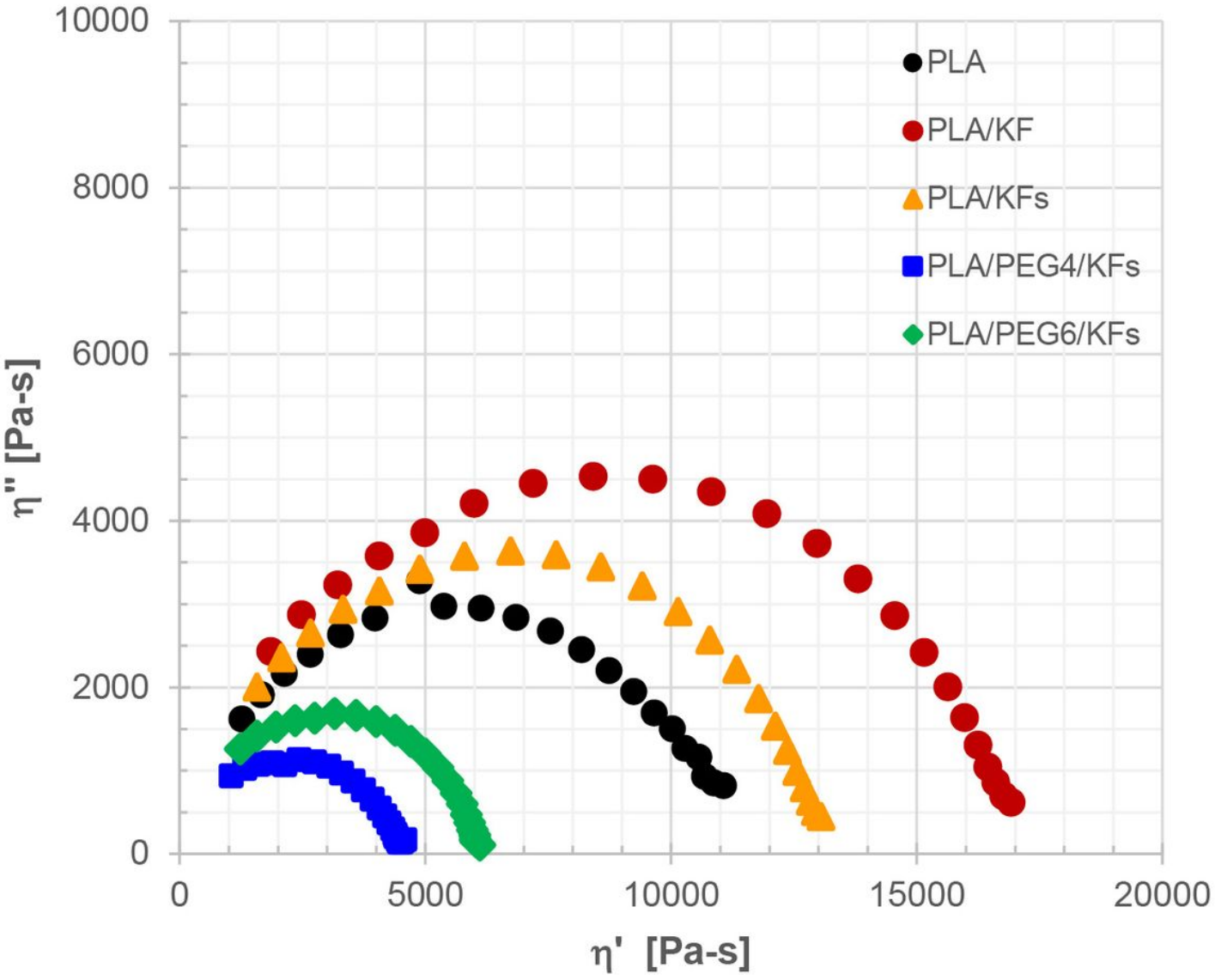

Figure 6

Cole-Cole plots of dynamic viscosity of PLA and its biocomposite filaments.

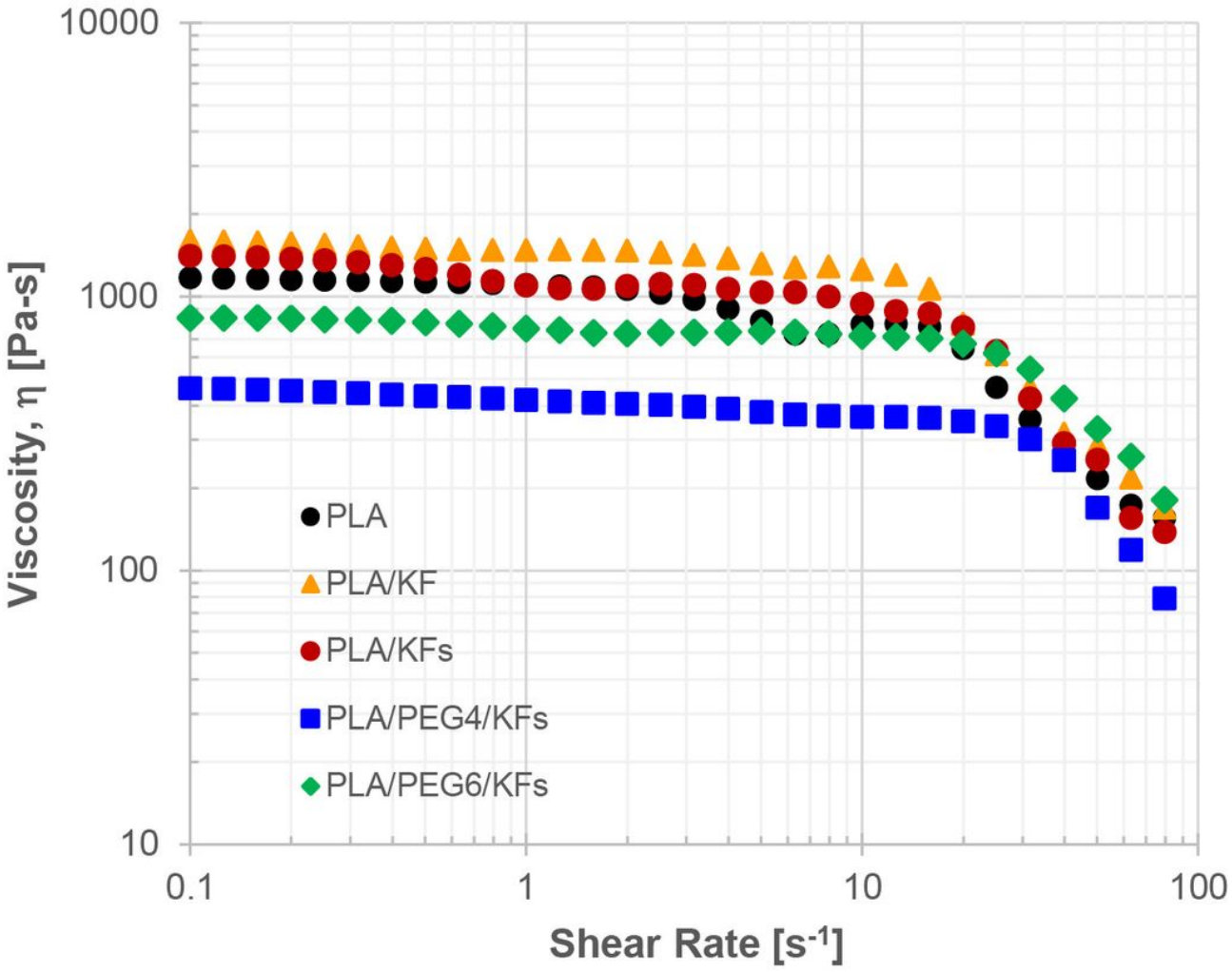

Figure 7

Steady shear viscosity as a function of shear rate for PLA and its biocomposite filaments.

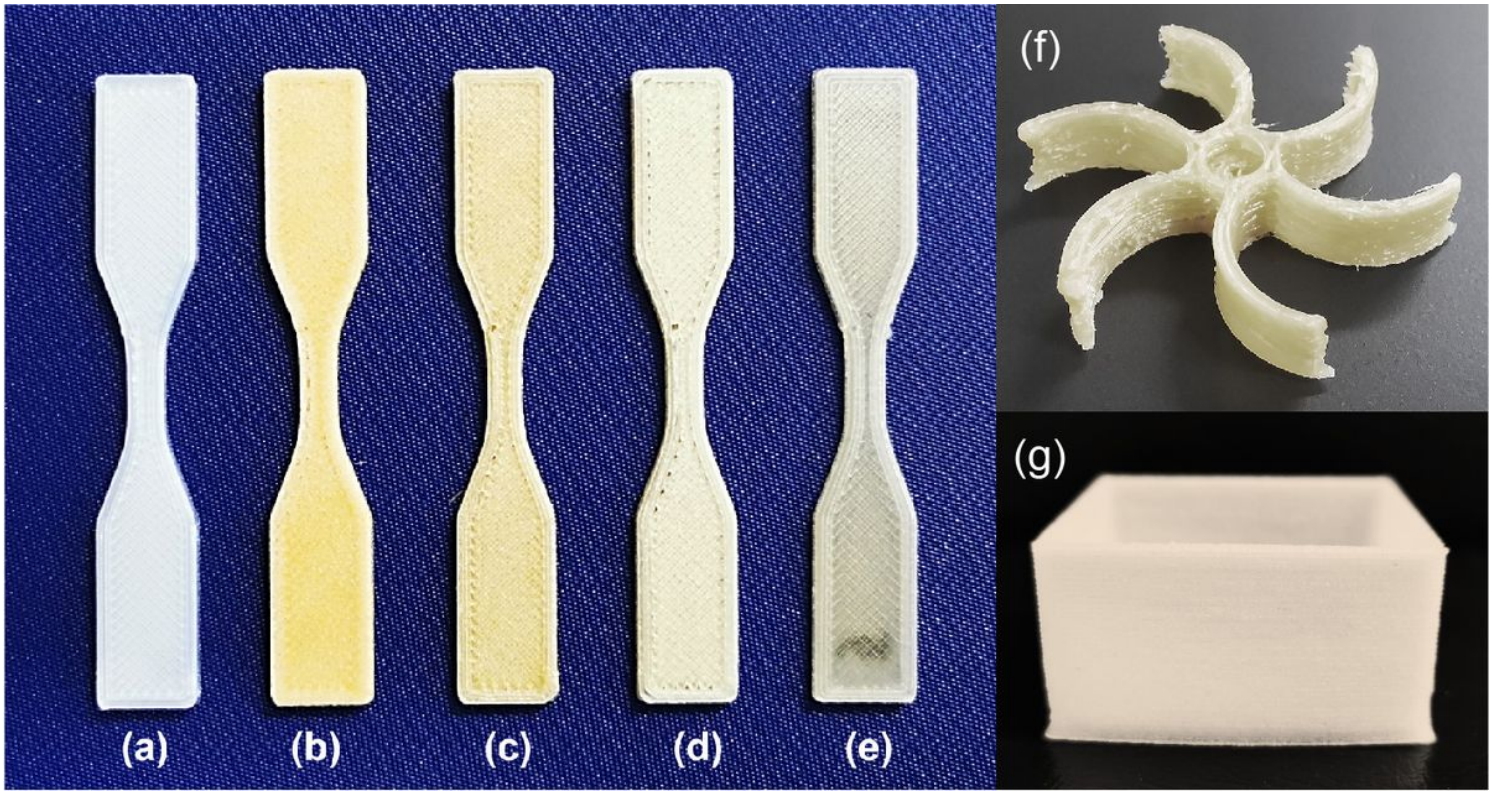

Figure 8

3D printed specimens of (a) PLA, (b) PLA/KF, (c) PLA/KFs, (d) PLA/PEG4/KFs, (e-g) PLA/PEG6/KFs.

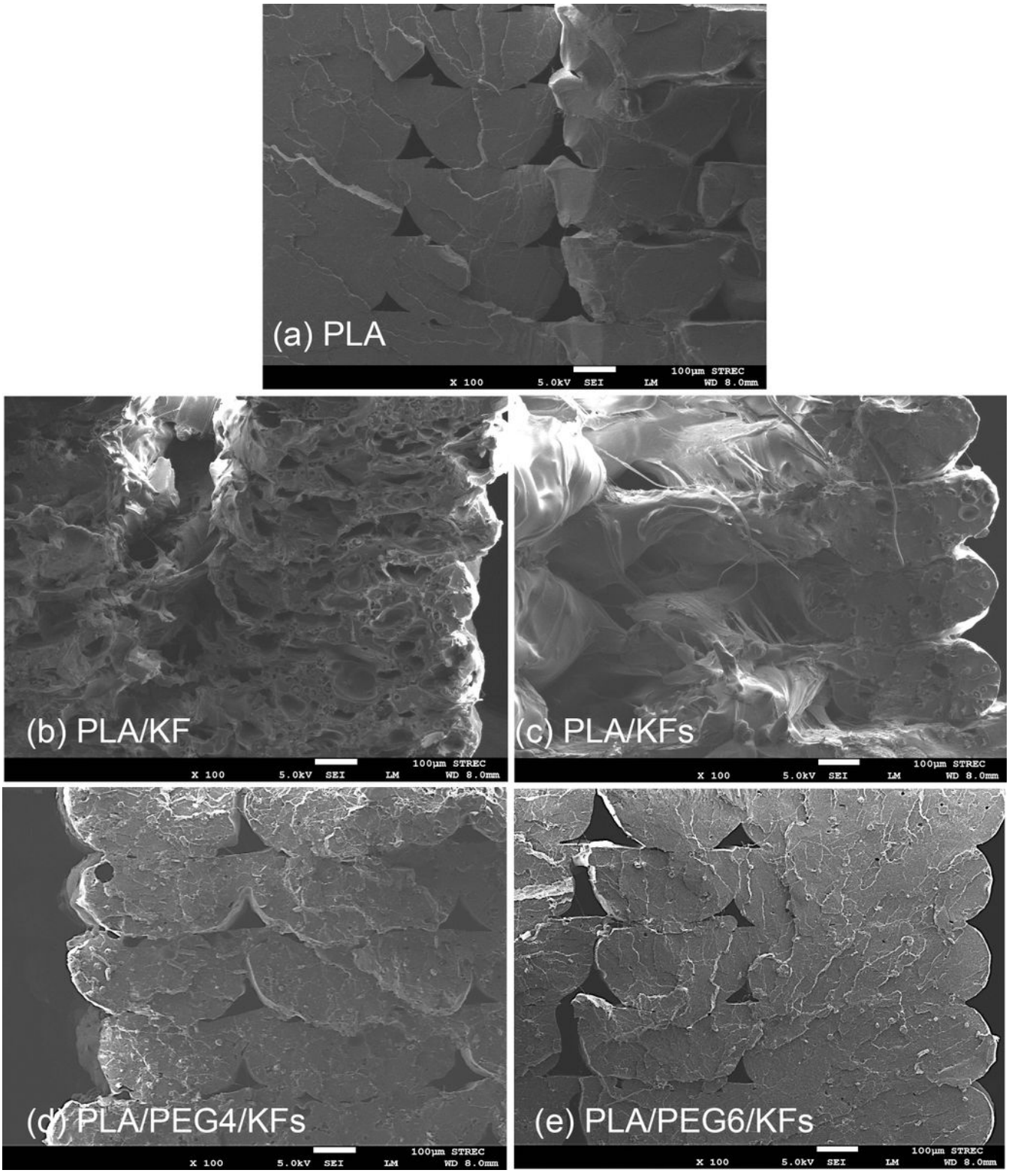

Figure 9

SEM images of the printed samples from (a) PLA, (b) PLA/KF, (c) PLA/KFs, (d) PLA/PEG4/KFs and (e) PLA/PEG6/KFs biocomposites at 100x magnification.

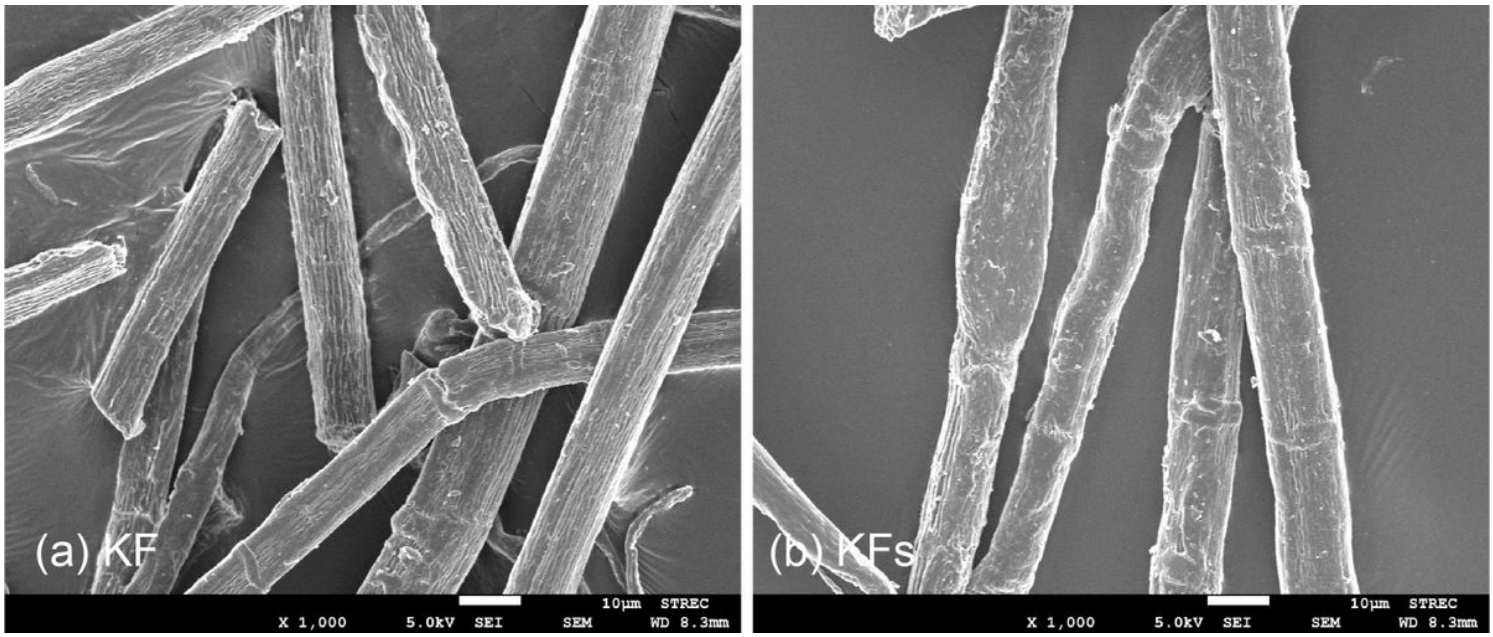

Figure 10

. SEM images of (a) kenaf cellulose fiber (KF) and (b) TEOS modified kenaf cellulose fiber (KFs) at 1000x magnification.

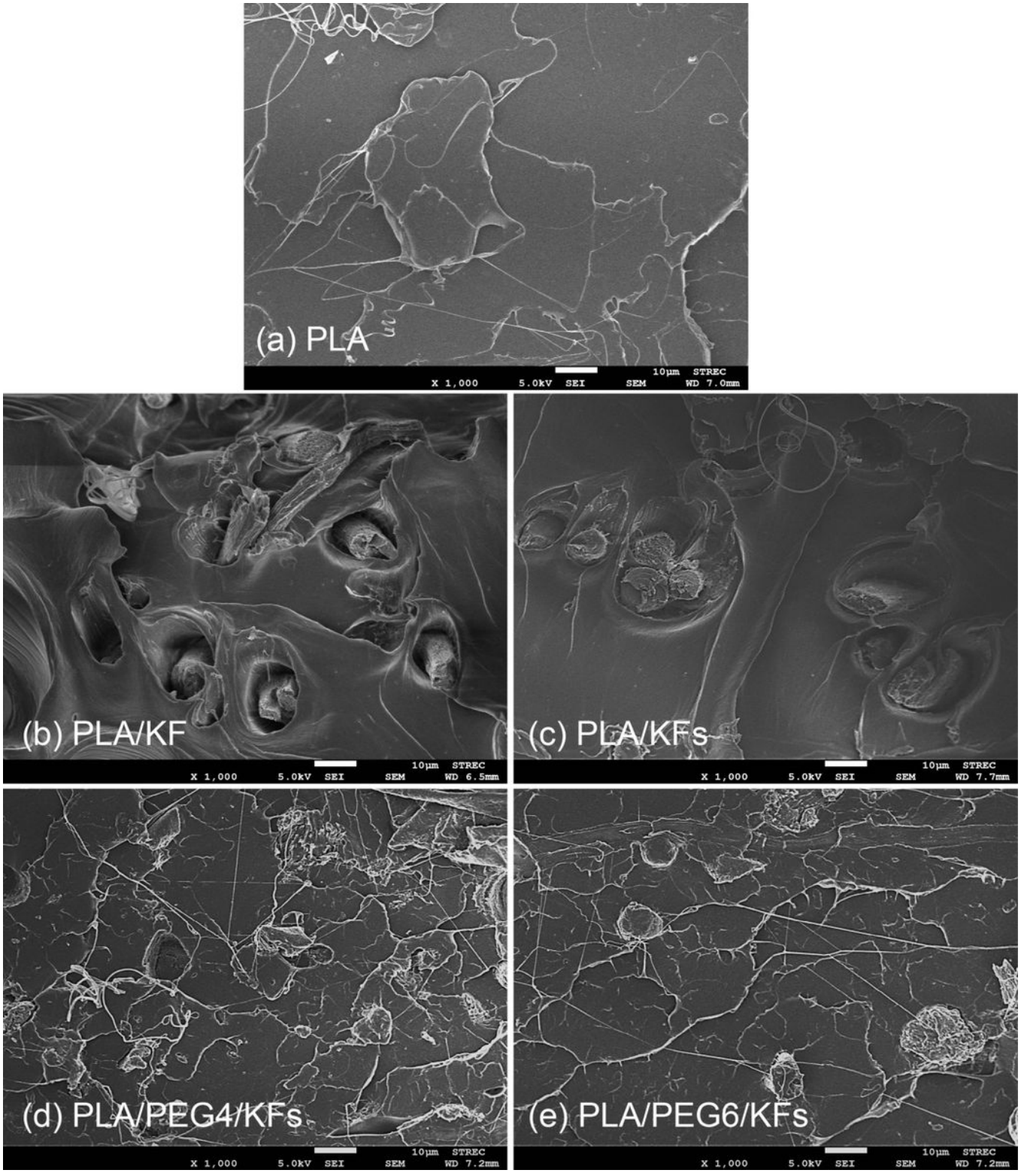

Figure 11

SEM images of the printed samples from (a) PLA; (b) PLA/KF; (c) PLA/KFs; (d) PLA/PEG4/KFs and (e) PLA/PEG6/KFs biocomposites at 1000x magnification.

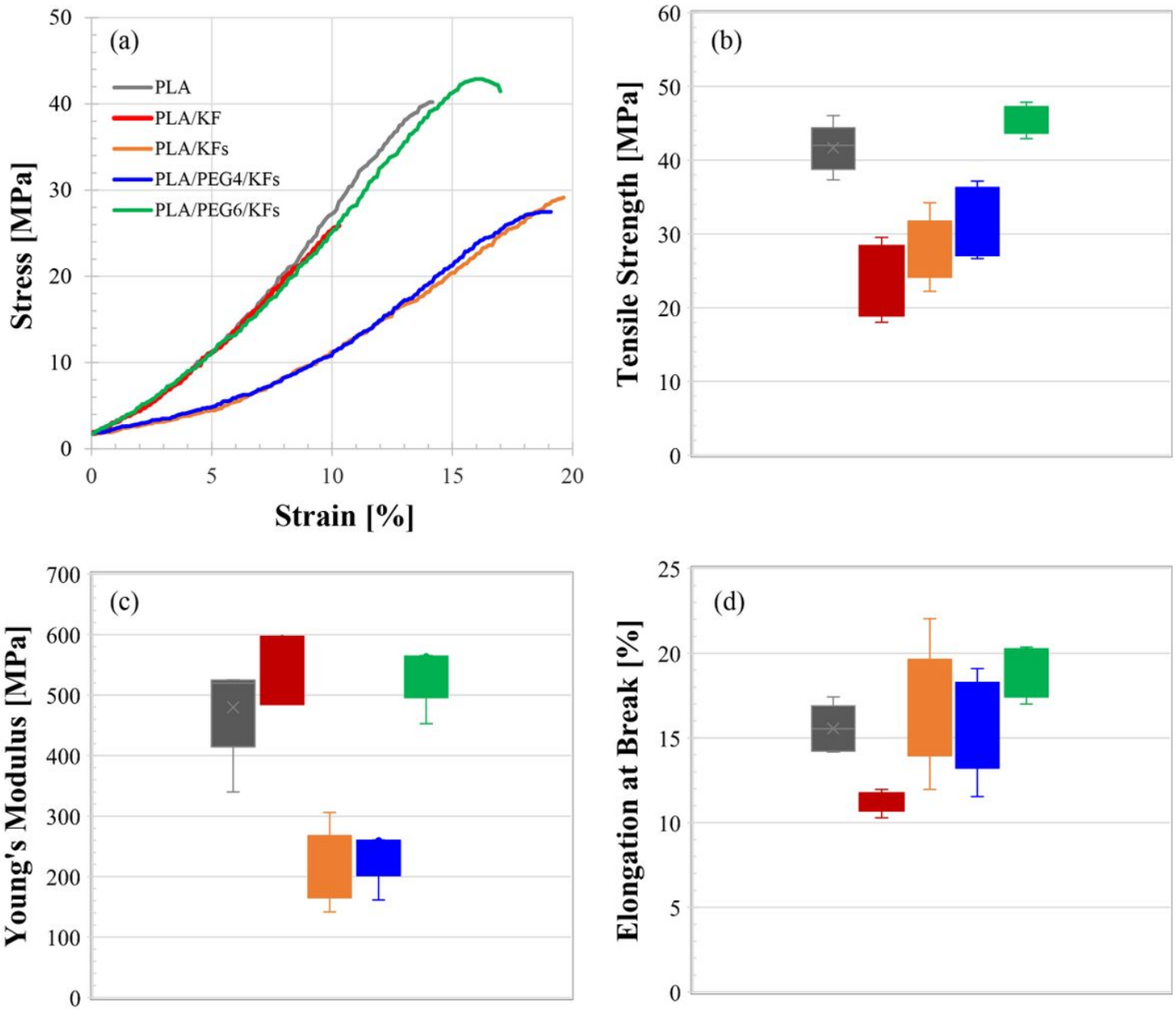

Figure 12

Tensile properties of PLA and PLA/kenaf cellulose fiber composites: (a) stress-strain curves, and box-whisker plots of (b) tensile strength, (c) Young's modulus and (d) elongation at break.